The 6th International Supercritical CO_2 Power Cycles Symposium
March 27 - 29, 2018, Pittsburgh, Pennsylvania

Comparison of Grade 91 and 347H Corrosion Resistance of Low-Temperature Components in Direct Supercritical CO_2 Power Cycles

Reyixiati Repukaiti
Graduate Teaching Assistant
Oregon State University
Corvallis, OR USA
repukair@oregonstate.edu

Lucas Teeter
Graduate Research Assistant
Oregon State University
Corvallis, OR USA
teeterl@oregonstate.edu

Margaret Ziomek-Moroz
Research Chemist
National Energy Technology Laboratory
Albany, OR USA
margaret.ziomek-moroz@netl.doe.gov

Ömer N. Doğan
Materials Research Engineer
National Energy Technology Laboratory
Albany, OR USA
omer.dogan@netl.doe.gov

Randal B. Thomas
Research Scientist
National Energy Technology Laboratory and
AECOM
Albany, OR USA
randal.thomas@netl.doe.gov

Nicolas J. Huerta
Research Scientist
National Energy Technology Laboratory
Albany, OR USA
nicolas.huerta@netl.doe.gov

Julie D. Tucker
Assistant Professor
Oregon State University
Corvallis, OR 97330, USA
julie.tucker@oregonstate.edu

ABSTRACT

Material performance in low temperature components (e.g., heat exchangers) of the natural gas- and coal-fired direct supercritical CO_2 power cycle systems is a concern because a highly corrosive environment is formed when aqueous condensation takes place in water saturated CO_2. The corrosion behavior of Grade 91 and 347H steels was investigated in oxygenated water saturated with CO_2 at 8 MPa and 50°C, 100°C, 150°C and 245°C. Both Grade 91, a ferritic-martensitic steel, and 347H, an austenitic stainless steel, are used in manufacturing heat exchangers.

Quantification of corrosion and the morphology of passive films and their chemical composition were determined. Mass loss measurements were used to determine corrosion rates. Characterization of the corrosion products was performed using light optical and scanning electron microscopy, energy dispersive X-ray spectroscopy and X-ray diffraction. The results indicate that at all temperatures investigated, the corrosive carbonic acid environment of the condensate inside a heat exchanger would cause significant corrosion on Grade 91 steel forming a non-protective oxide film. This contrasts with results for 347H which forms a stable passive film resulting in minimal corrosion in conditions expected inside a heat exchanger of a direct cycle power plant.

INTRODUCTION

Power generation using fossil fuel-fired direct supercritical CO_2 (sCO_2) cycles is a developing technology that is expected to improve power generation efficiency and reduce emissions without increasing cost of electricity [1]. However, there are challenges unique to this technology. One of these challenges is the low-temperature corrosion of materials in parts such as low-temperature recuperator and cooler. Water dissolved in sCO_2 at high temperatures begins to condense to an aqueous phase with dissolved CO_2 as temperature of the working fluid decreases. Since the condensing water is saturated with CO_2 (essentially carbonic acid), aqueous corrosion is observed on the surface of steels [2, 3]. The corrosion is severe on the lower Cr containing steels such as Grades 91 and 22 which are traditionally used for lower temperature applications in steam cycles. As a result, higher cost austenitic stainless steels are proposed to be used in fabrication of lower temperature heat exchangers resulting in higher capital cost. This paper discusses corrosion behavior of two steels (Grade 91 and 347H) in sCO_2 environment containing H_2O and O_2 at 8 MPa pressure and temperature range from 50°C to 245°C.

MATERIALS AND METHODS

Grade 91 ferritic-martensitic steel and 347H austenitic stainless steel were used in this research. The chemical compositions are listed in Table 1 as provided by the manufacturer (Arcellor Mittal). The 347H plate was in solution annealed state and the Grade 91 plate was normalized (1038°C), tempered (788°C), and air cooled.

Table 1: Alloy chemical composition (wt%)

Alloy	Description	Cr	Ni	C	Mn	P	S	Si	Co	Cu	Mo	N	Nb	Fe
347H	Austenitic stainless steel	17.3	9.09	0.05	1.5	0.03	0.01	0.38	0.16	0.43	0.41	0.04	0.62	Bal.
Gr 91	Martensitic-ferritic steel	8.37	0.09	0.09	0.45	0.01	0.01	0.33	-	0.09	0.9	0.045	0.07	Bal.

All samples were machined from plates into coupons with dimensions of 20 mm x 25 mm x 6 mm with a 6 mm diameter hole. The coupons were lapped with alumina slurry, and then ground and polished with SiC abrasive paper to 1200 grit. Afterwards, the coupons were cleaned with deionized water and in ultrasonic bath with isopropanol solution for 30 seconds. Finally, samples were rinsed with deionized water and fast dried with air.

The coupons of each alloy were all exposed in autoclaves in a mixture fluid of CO_2-H_2O-O_2 at 8 MPa and temperatures of 50°C, 100°C, 150°, and 245°C. Each test condition had 6 coupons except 50°C had 4 coupons. The environment was created by filling 750 ml deionized water into 1100 ml autoclave, as illustrated in Figure 1. All coupons were completely submerged in the water phase. Then the headspace was flushed with argon (99.999% purity) and then with a gas mix of 99%CO_2 and 1%O_2. Eventually, the temperature and pressure were increased to set points simultaneously with CO_2 and O_2 gas mixture. Tests duration was 500 hours. During the shutdown period, temperature and pressure were decreased simultaneously and gradually to room temperature and ambient pressure.

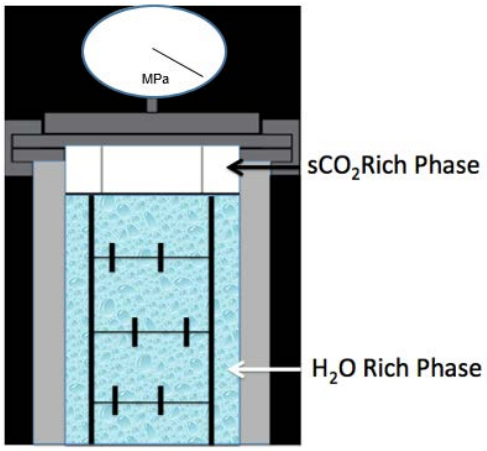

Figure 1: Exposure experiment setup

The exposed coupons were weighed using a balance capable of measuring 10^{-5} grams to determine the mass change. X-ray diffraction (XRD) was used in the glancing-angle mode to determine the compounds forming on the surface of the coupons due to exposure. The XRD apparatus was a Rigaku Ultima III. Copper Kα characteristic radiation was used to scan a 2Θ range of 10° to 100° with a 0.02° step size. An FEI Inspect scanning electron microscope was used to obtain images of the exposed surfaces in secondary electron mode.

RESULTS AND DISCUSSION

The exposure conditions (P and T) used in this study are shown on the H_2O and CO_2 phase diagrams in Figures 2 and 3 [4], respectively. While any water that is not dissolved in the CO_2 phase is present in liquid form, the CO_2 is in supercritical form under the experimental conditions, as shown in the figures.

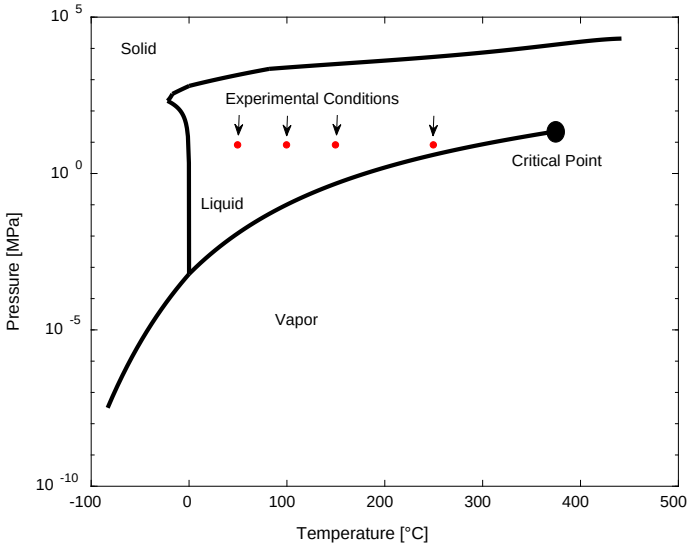

Figure 2: H_2O phase diagram showing the experimental phase region.

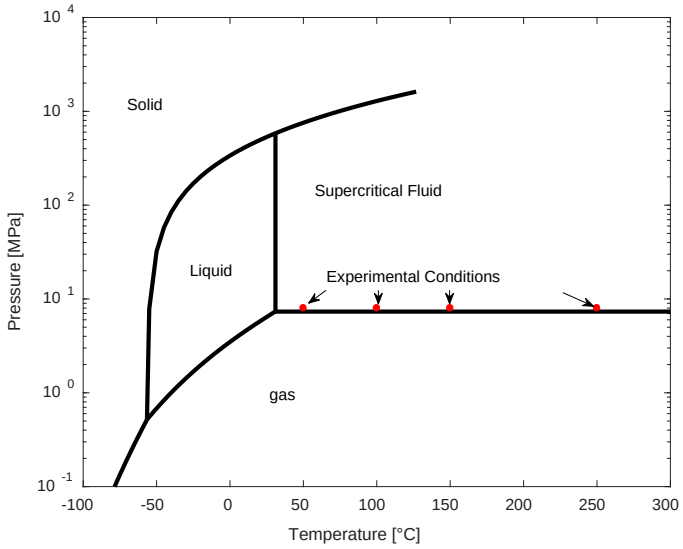

Figure 3: CO_2 phase diagram showing the experimental phase region

Since coupons were submerged in the liquid H_2O phase, the solubility of CO_2 and O_2 in H_2O has significant impact on the alloys' corrosion behavior at the test conditions. Solubility of CO_2 in H_2O as a function of temperature and pressure is displayed in Figure 4 [5]. The figure shows that the mole fraction of CO_2 in pure water decreases as the temperature increases at 5 and 10 MPa. However, when pressure is 20 MPa, CO_2 mole fraction hits a minimum value when temperature reaches approximately 80°C, and then the value would increase as temperature increases. In the present research, the test pressure is 8 MPa. The solubility of CO_2 in H_2O can be extrapolated from the graph (Fig. 4). Therefore, CO_2 mole fraction should decrease as the temperature increases.

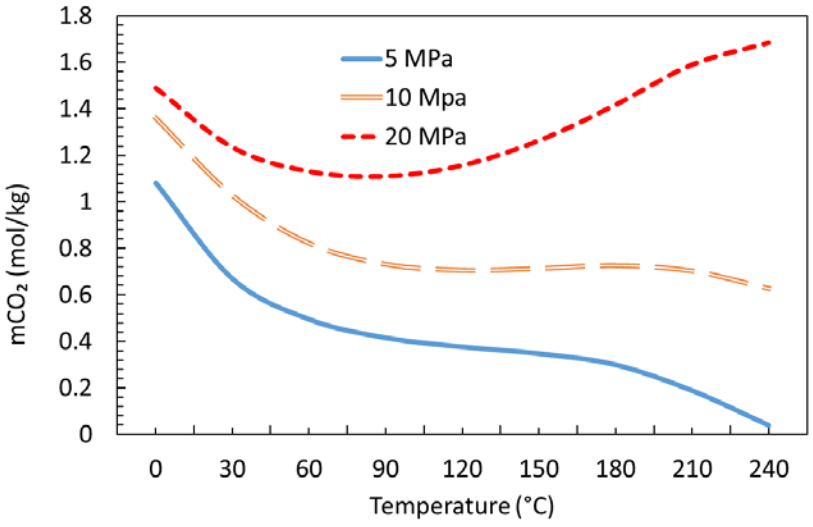

Figure 4: Solubility of CO_2 in pure H_2O as functions of temperature and pressure.

Oxygen solubility in aqueous H_2O varies with pressure and temperature as well. According to Geng et al. [6], O_2 mole fraction in H_2O reaches a stable value around 0.03 mol/kg at 5 MPa (Figure 5). However, when pressure is at 10 or 20 MPa, O_2 solubility would increase after it hits a minimum value at 90°C approximately. O_2 solubility has different characteristics functions at 5 and 10 MPa, thus it is difficult to extrapolate the O_2 solubility at 8 MPa, but the solubility value should be lower than 0.15 mol/kg and higher than 0.04 mol/kg at all temperatures selected for the experiments. This indicates that there is enough

oxygen available for a cathodic reaction during the corrosion process. However, the interaction of mutually dissolved CO_2 and O_2 could affect each other's solubility, more studies are ongoing.

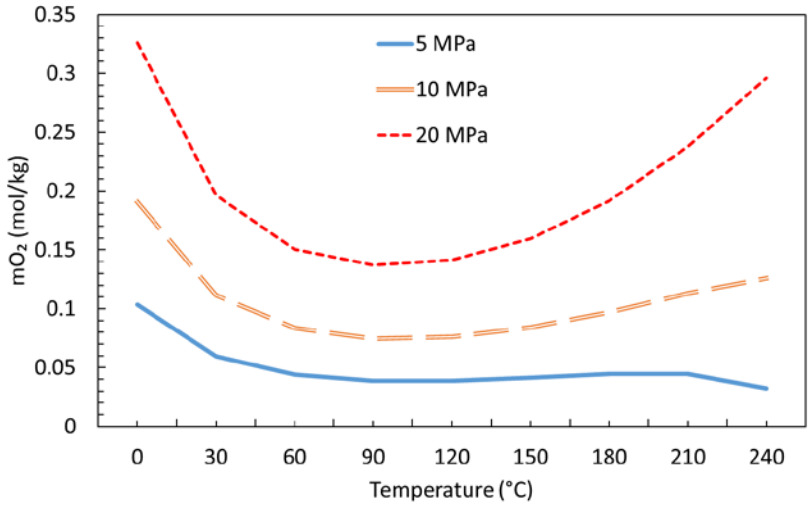

Figure 5: Solubility of O_2 in pure water as functions of temperature and pressure

Weight measurement data for the corroded 347H and Grade 91 are shown in Figure 6. Grade 91 lost mass at all four temperatures due to detachment of corrosion products from the surface of coupons. The results show that Grade 91 lost more mass as a result of corrosion in water rich phase at lower temperatures (50 and 100°C). This is related to the solubility of CO_2 in water. As the temperature decreases, the solubility of CO_2 in water increases, making the solution more acidic (Figure 4). On the other hand, oxygen solubility in water does not change significantly at 8 MPa at the exposure temperature range (Figure 5). It was observed that the mass loss of Grade 91 at 50°C was less than that at 100°C even though the solution was expected to be more acidic at 50°C. This was attributed to the slower corrosion kinetics at 50°C even though the driving force for corrosion was greater. Comparing to Grade 91, the mass change for 347H was minimal at all four temperatures (Figure 6). No conclusive mass change trend can be established for 347H due to the large error bars. 347H's corrosion resistance had little change throughout the temperature range.

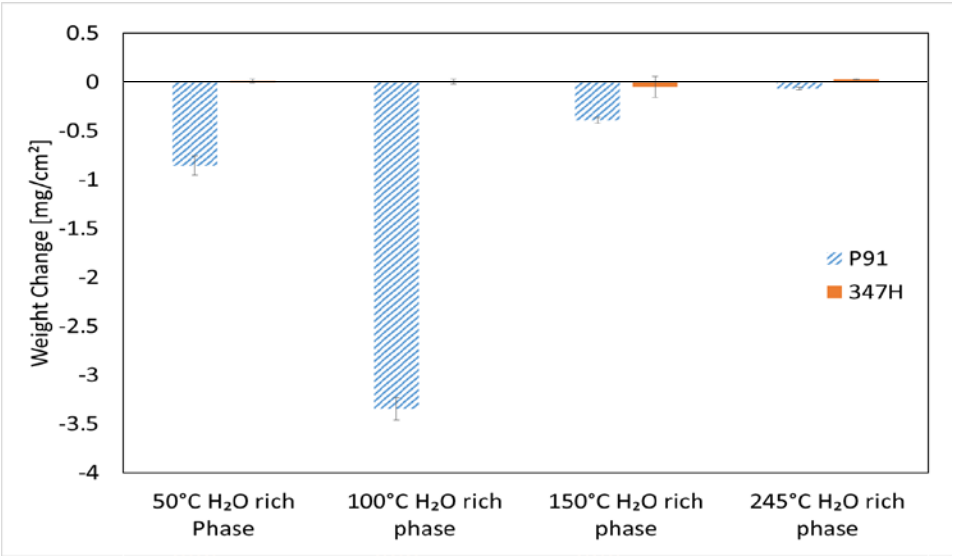

Figure 6: Weight change of alloys as a result of exposure testing

Although most of the corrosion products forming on the Grade 91 coupons detached from the surface, the

SEM investigation revealed the presence of residual corrosion products on the coupon surfaces, Figure 7. The corrosion products were scattered on the surface in powder (spongy) shape. Furthermore, cracks were observed in the residual corrosion layer and local spallation was visible on the samples that were immersed in H_2O rich phase at 150°C (Fig. 7c) and 245°C (Fig. 7d). These cracks may be caused by shrinkage of the corrosion products during drying or de-hydration.

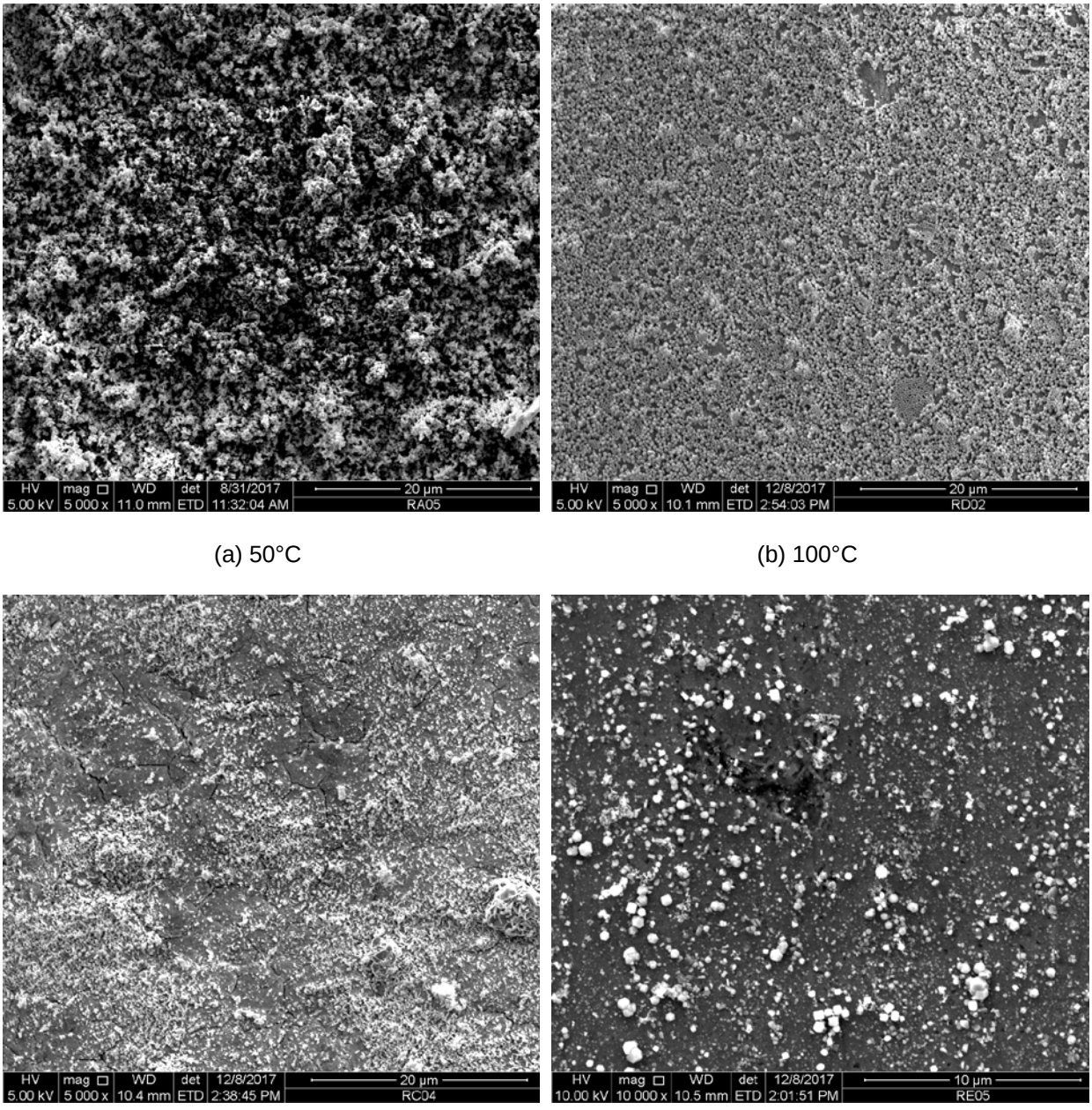

(a) 50°C (b) 100°C

(c) 150°C (d) 245°C

Figure 7: Secondary electron SEM images of P91 after exposure tests

The 347H coupons did not show much corrosion products on their surfaces, Figure 8. No corrosion products were observed on the surfaces except for the coupons that were immersed in the H_2O rich phase at 245°C. This SEM observation on the 245°C 347H coupons were also supported by the mass change data which showed a slight positive mass change for 347H at 245°C. Further work is underway to explain this behavior.

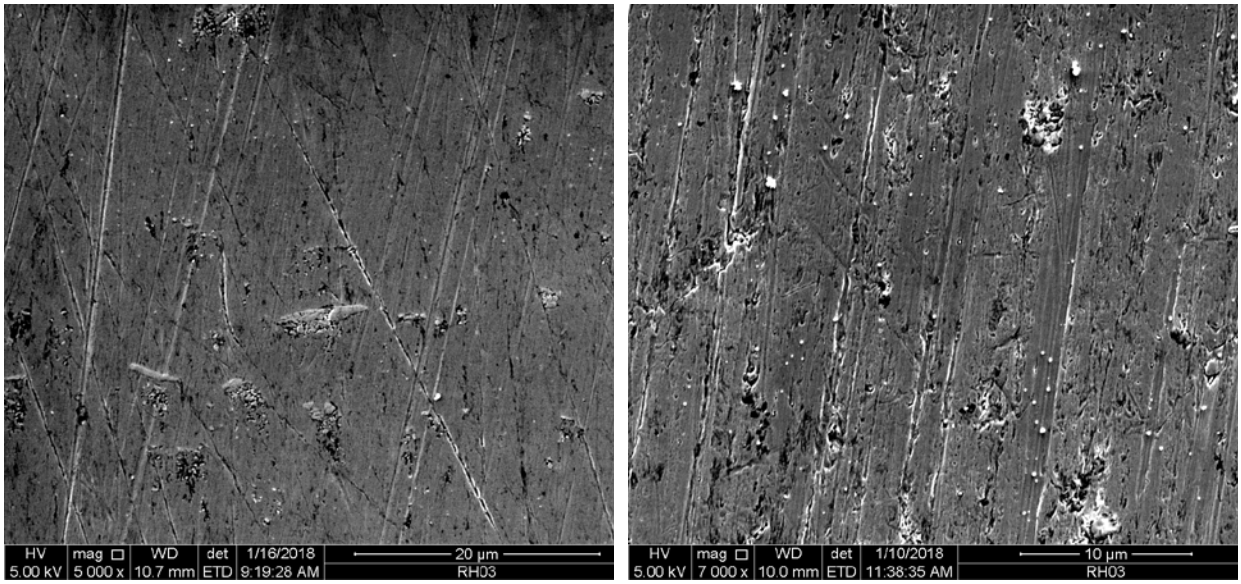

(a) 50°C (b) 100°C

(c) 150°C (d) 245°C

Figure 8: Secondary electron SEM images of 347H after exposure tests

Based on the XRD results for P91 shown in Table 2, Fe_2O_3 and Fe_3O_4 are the major corrosion products on samples in all conditions. They can form in following anodic electrochemical reactions (Eqs 1-2):

$$3Fe + 4H_2O = Fe_3O_4 + 8H^+ + 8e \quad \text{(Eq.1)}$$

$$Fe_3O_4 + H_2O = 3Fe_2O_3 + 2H^+ + 2e \quad \text{(Eq.2)}$$

The cathodic reaction is represented by the following reaction (Eq.3) since there is enough oxygen in the H_2O rich phase environment:

$$O_2 + 4H^+ + 4e = 2H_2O \quad \text{(Eq.3)}$$

The corrosion products are oxides indicating that oxygen is the primary oxidant in these environments. At

lower temperatures, more mass change and corrosion products were observed from weight measurement and SEM data, this phenomenon is due to a more acidic environment that accelerated the anodic reactions. 347H has very thin oxide layer, thus glancing angle XRD could not detect any oxide layer but base metal, and thus 347H XRD results are not included in this paper.

Table 2: Glancing angle XRD results of P91 corrosion products after exposure tests

Alloy	50°C	100°C	150°C	245°C
Gr 91	Fe_2O_3 FeO(OH) Fe_3O_4	Fe_2O_3 Fe_3O_4	Fe_2O_3 Fe_3O_4	Fe_2O_3 Fe_3O_4

These results are consistent with those reported earlier [7]. In that study, at 25 °C and 50 °C, the carbonic acid caused more corrosion on Grade 91 than 347H, as demonstrated by the corrosion rates calculated from the electrochemical experiments. Based on the autoclave immersion tests, Grade 91 formed non-protective passive film resulting in significant corrosion while 347H formed a stable passive film resulting in minimal corrosion.

CONCLUSIONS

Multiple conclusions can be drawn from this work by comparing 347H and Grade 91's mass change and corrosion products.

- More mass change was observed on the Grade 91 coupons after the 500-hour exposures at 8 MPa at all four temperatures between 50°C and 245°C than mass change of 347H. The mass loss at lower temperatures (50°C and 100°C) was greater due to the higher CO_2 solubility in water that contributed to the anodic reactions.
- Residual corrosion products on the Grade 91 coupons were identified as Fe_2O_3 and Fe_3O_4.
- 347H coupons showed minimal mass change and very thin passive layers.
- The results of this study indicate that the lower Cr steels such as Grade 91 may not be suitable for the low / intermediate temperature components in the direct sCO_2 power cycles.

ACKNOWLEDGEMENTS

This work was performed in support of the U.S. Department of Energy's Fossil Energy Crosscutting Technology Research and Advanced Turbine Programs. The Research was executed through NETL Research and Innovation Center's Advanced Alloy Development Field Work Proposal. This research was supported in part by an appointment (RR and LT) to the NETL Research Participation Program sponsored by the U.S. Department of Energy and administered by the Oak Ridge Institute for Science and Education. The authors thank Mr. Jeffrey Oberfoell for performing the autoclave tests. Discussions with Dr. Xijia Lu of 8 Rivers Capital were appreciated.

REFERENCES

[1] Weiland, N.T., Dennis, R.A., Ames, R., Lawson, S., Strakey, P., Chapter 12 “Fossil Energy” in Fundamentals and Applications of Supercritical Carbon Dioxide Based Power Cycles, Eds. K. Brun, P. Friedman, R. Dennis, Woodhead Publishing, 2017.

[2] Teeter, L., Huerta, N., Doğan, Ö ., Ziomek-Moroz, M., Oleksak, R., Oryshchyn, D., ... & Tucker, J.. Corrosion Behavior of Austenitic Stainless Steel in Supercritical CO_2 Containing O_2 and H_2O. 2016 ECS Transactions, 72(17), 137-148.

[3] Repukaiti, R., Teeter, L., Ziomek-Moroz, M., Doğan, Ö., & Tucker, J. Corrosion Behavior of Steels in Supercritical CO_2 for Power Cycle Applications. 2017, ECS Transactions, 77(11), 799-808.

[4] Huber, K. P., and G. Herzberg. "NIST Standard Reference Database, Material measurement laboratory, Data Gateway." 1977, Chemistry WebBook. Data collected.

[5] Duan, Z., & Sun, R. An improved model calculating CO_2 solubility in pure water and aqueous NaCl solutions from 273 to 533 K and from 0 to 2000 bar. 2003, Chemical Geology, 193(3), 257-271.

[6] Geng, M., & Duan, Z.. Prediction of oxygen solubility in pure water and brines up to high temperatures and pressures. 2010, Geochimica Et Cosmochimica Acta, 74(19), 5631-5640.

[7] Repukaiti, R., Teeter, L., Ziomek-Moroz, M., Doğan, Ö., Huerta, N., Thomas, R., & Tucker, J. Corrosion Behavior of an Austenitic Stainless Steel and a Martensitic-Ferritic Steel in Direct Supercritical CO_2 Power Systems. 2018, Corrosion 2018, Manuscript accepted.